AGU PUBLICATIONS

Global Biogeochemical Cycles

RESEARCH ARTICLE
10.1002/2016GB005426

Key Points:
- Uncertainty in ocean carbon uptake projections is quantified and partitioned
- Emission scenario dominates uncertainty in globally integrated carbon uptake projections
- Internal variability and model structure dominate uncertainty on regional scales

Correspondence to:
N. S. Lovenduski,
nicole.lovenduski@colorado.edu

Citation:
Lovenduski, N. S., G. A. McKinley, A. R. Fay, K. Lindsay, and M. C. Long (2016), Partitioning uncertainty in ocean carbon uptake projections: Internal variability, emission scenario, and model structure, *Global Biogeochem. Cycles*, *30*, 1276–1287, doi:10.1002/2016GB005426.

Received 11 APR 2016
Accepted 8 AUG 2016
Accepted article online 11 AUG 2016
Published online 1 SEP 2016

Partitioning uncertainty in ocean carbon uptake projections: Internal variability, emission scenario, and model structure

Nicole S. Lovenduski[1], Galen A. McKinley[2], Amanda R. Fay[2], Keith Lindsay[3], and Matthew C. Long[3]

[1]Department of Atmospheric and Oceanic Sciences and Institute of Arctic and Alpine Research, University of Colorado Boulder, Boulder, Colorado, USA, [2]Department of Atmospheric and Oceanic Sciences, University of Wisconsin-Madison, Madison, Wisconsin, USA, [3]Climate and Global Dynamics Laboratory, National Center for Atmospheric Research, Boulder, Colorado, USA

Abstract We quantify and isolate the sources of projection uncertainty in annual-mean sea-air CO_2 flux over the period 2006–2080 on global and regional scales using output from two sets of ensembles with the Community Earth System Model (CESM) and models participating in the 5th Coupled Model Intercomparison Project (CMIP5). For annual-mean, globally-integrated sea-air CO_2 flux, uncertainty grows with prediction lead time and is primarily attributed to uncertainty in emission scenario. At the regional scale of the California Current System, we observe relatively high uncertainty that is nearly constant for all prediction lead times, and is dominated by internal climate variability and model structure, respectively in the CESM and CMIP5 model suites. Analysis of CO_2 flux projections over 17 biogeographical biomes reveals a spatially heterogenous pattern of projection uncertainty. On the biome scale, uncertainty is driven by a combination of internal climate variability and model structure, with emission scenario emerging as the dominant source for long projection lead times in both modeling suites.

1. Introduction

Since the beginning of the industrial revolution, atmospheric concentrations of carbon dioxide (CO_2) have increased by 40%, driving increases in global temperature [*Ciais and Sabine*, 2013]. Less than half of the CO_2 emitted from anthropogenic activities has remained in the atmosphere; the remaining CO_2 has been taken up by natural carbon sinks: the ocean and the terrestrial biosphere. The global ocean has absorbed ~30% of the CO_2 released by fossil fuel burning, cement manufacture, and land use since 1765 [*Ciais and Sabine*, 2013]. Accurate projections of future climate change require quantitative projections of CO_2 uptake by the ocean.

Earth System Model (ESM) simulations project the future evolution of ocean carbon uptake on timescales ranging from subannual to centennial. However, quantitative projections from ESMs across these timescales are subject to considerable uncertainty, particularly at regional scales [*Roy et al.*, 2011; *Friedrich et al.*, 2012; *Frölicher et al.*, 2014; *Tjiputra et al.*, 2014; *Hauck et al.*, 2015; *Laufkötter et al.*, 2015]. If ESMs are to be used to quantify future changes in ocean carbon uptake across these timescales and at regional spatial scales, their uncertainties must be well known and well understood. *Hawkins and Sutton* [2009] describe three main types of projection uncertainty:

1. *Uncertainty due to internal variability.* Internal variability is the unforced climate variability that arises from natural internal processes within the climate system. In the tropics, the dominant mode of internal climate variability is the El Niño–Southern Oscillation. In the extratropics, internal variability is characterized by several major climate modes: the North Atlantic Oscillation, Atlantic Multidecadal Oscillation, Pacific Decadal Oscillation, and Southern Annular Mode (SAM), to name a few. Internal variability has the potential to dampen or amplify—for a few years to several decades—the long-term trends in ocean carbon uptake that are associated with anthropogenic CO_2 emissions. For example, on the basis of a model hindcast simulation, *Lovenduski et al.* [2015a] find that periods with positive trends in the SAM are associated with a temporary weakening of the Southern Ocean CO_2 sink.
2. *Uncertainty due to emission scenario.* Future emissions of greenhouse gases will drive changes in the ocean carbon sink, ultimately determining future radiative forcing and climate. However, future emissions are highly uncertain, given our inability to project the complex changes in society and technology upon which they depend. As a result, future simulations are conducted for "scenarios," spanning a range of forcing

intensity and climate outcomes. For instance, modeling centers participating in the 5th Coupled Model Intercomparison Project (CMIP5) were requested to simulate the future climate under four Representative Concentration Pathway (RCP) emission scenarios: RCP2.6, RCP4.5, RCP6.0, and RCP8.5 [*Meinshausen et al.*, 2011]. Projections of future ocean carbon uptake from ESMs are greatly influenced by the choice of emission scenario. For example, the cumulative oceanic storage of anthropogenic carbon in CMIP5 models by 2100 ranges from 110–220 Pg C under RCP2.6 to 320–635 Pg C under RCP8.5 [*Ciais and Sabine*, 2013].

3. *Uncertainty due to model structure.* Model structure is a catch-all term used to describe how the physical world is represented in an ESM, including the mathematical expressions, numerical methods, and parameterizations employed in that representation. Model structure determines the behavior of the model, leading to differing climate sensitivities and carbon-climate feedbacks. These structural differences yield different climate change responses to the same radiative forcing; different carbon cycle responses result from different climates and structural differences between the carbon cycle formulations. For example, the CMIP5 model simulations run under RCP8.5 project a wide range of cumulative anthropogenic carbon storage by 2100 (320–635 Pg C) [*Ciais and Sabine*, 2013] due to both internal variability and structural uncertainty. Analysis of carbon feedbacks from a coordinated set of ESM experiments run under a 1% per year CO_2 increase suggests that some fraction of this spread is due to the different formulations of the carbon cycle models in CMIP5 [*Arora et al.*, 2013], with the remaining structural uncertainty driven by the physical climate system.

On the basis of surface air temperature projections in CMIP3 models, *Hawkins and Sutton* [2009] show that the fractional contribution of the three sources of uncertainty varies with prediction lead time and spatial averaging scale. Their results suggest that on the global scale, model structure and internal variability dominate the surface air temperature projection uncertainty for short lead times (<50 years), whereas the emission scenario is the primary source of projection uncertainty for long lead times (>50 years), reflecting spread across the SRES A2, A1B, and B1 scenarios. Total projection uncertainty at regional scales is higher than on the global scale, with large contributions from internal variability and model structure for all prediction lead times [*Hawkins and Sutton*, 2009]. While not yet partitioned and described in the literature, these same sources of uncertainty impact model projections of sea-air CO_2 flux. Here we isolate and quantify the evolution of the three sources of sea-air CO_2 flux projection uncertainty on global and regional scales using output from multiple ESM simulations of future climate.

Numerous studies suggest that the use of a large ensemble of simulations from a single climate model is key to estimating uncertainty in regional-scale climate change projections [see *Deser et al.*, 2016, and references therein]. Such ensembles typically include ~30 members, each of which is subject to an identical external forcing but starts from a slightly different atmospheric or oceanic state. While it has become fairly common practice to use a large ensemble of simulations to estimate projection uncertainty in the atmospheric physical state, the use of large ensembles has just begun to gain traction in the ocean biogeochemical community [*Frölicher et al.*, 2009; *Rodgers et al.*, 2015; *McKinley et al.*, 2016; *Long et al.*, 2016; *Frölicher et al.*, 2016]. Large ensembles are computationally expensive, and the computational cost can increase significantly for simulations that include tracers for ocean biogeochemistry. Here we make use of output from two sets of ensembles using the Community Earth System Model (CESM) with fully resolved ocean carbon and biogeochemistry. The first, the CESM Large Ensemble (CESM-LE), simulates the period 1920–2100 with 38 members under historical and RCP8.5 external forcing [*Kay et al.*, 2015]. The second, the CESM Medium Ensemble (CESM-ME), simulates the period 2006–2080 with 15 members under RCP4.5 external forcing [*Sanderson et al.*, 2015]. Here we analyze annual-mean sea-air CO_2 flux over 2006–2080 in both CESM ensembles and in the CMIP5 models to quantify the uncertainty in CO_2 flux projections.

2. Modeling Methods

2.1. The CESM Ensembles

The CESM ensembles were conducted with CESM version 1, a configuration consisting of atmosphere, ocean, land, and sea ice component models [*Danabasoglu et al.*, 2012; *Lawrence et al.*, 2012; *Hunke and Lipscomb*, 2008; *Holland et al.*, 2012]. The ocean model has nominal 1° horizontal resolution and 60 vertical levels. Mesoscale eddy transport is parameterized with an updated version of *Gent and McWilliams* [1990], where the eddy-induced advection coefficient, κ, is diagnosed as a function of space and time. Diapycnal mixing is represented using the K-Profile Parameterization of *Large et al.* [1994], and mixed layer restratification

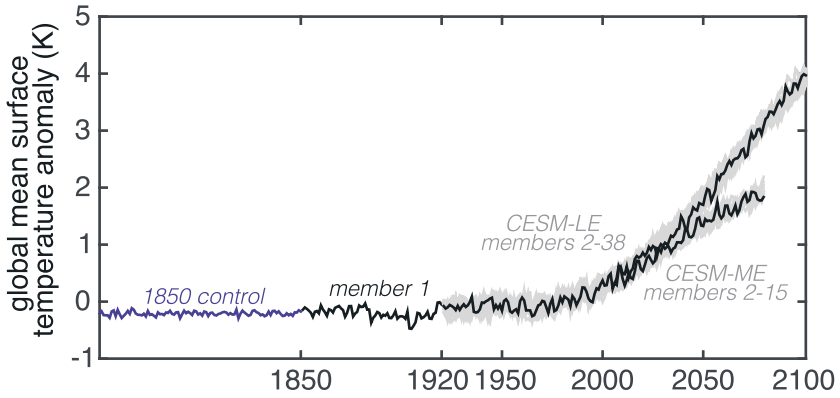

Figure 1. Annual-mean, global-mean surface temperature anomaly (relative to 1961-1990 base period) for the 1850 control and individual ensemble members for the CESM-LE and CESM-ME ensembles. Adapted from *Kay et al.* [2015] and *Sanderson et al.* [2015].

by submesoscale eddies is parameterized using the method of *Fox-Kemper et al.* [2011]. The biogeochemical ocean model incorporates multinutrient colimitation with three explicit phytoplankton functional types [*Moore et al.*, 2004, 2013], full carbonate system thermodynamics, sea-air CO_2 fluxes, and a dynamic iron cycle [*Doney et al.*, 2006; *Moore and Braucher*, 2008]. Phytoplankton calcification is unaffected by variations in the saturation state of calcite or aragonite. For the CESM ensemble integrations, shortwave absorption in the ocean is computed using a specified chlorophyll climatology, rather than the prognostic field, thereby rendering the ocean biogeochemistry passive with respect to impacts on physical climate. Atmospheric CO_2 concentrations are prescribed in CESM-LE and CESM-ME; thus, ocean CO_2 fluxes do not feed back on the modeled climate.

As described in *Kay et al.* [2015] and *Sanderson et al.* [2015], the CESM ensembles began with an 1850 control simulation with constant preindustrial forcing (Figure 1). The ocean model physical state was initialized to observations for this integration, while the ocean biogeochemical fields were initialized to a state derived from a separate 600 year spin-up. The other component models were initialized from previous CESM1 simulations. The first ensemble member was initialized from a randomly selected year in the 1850 control run (year 402; Figure 1) and integrated forward from 1850 to 2100. The remaining CESM-LE ensemble members were integrated from 1920 to 2100 using initial conditions from 1 January 1920 in the first ensemble member plus round-off level ($\mathcal{O}(10^{-14})$ K) perturbations to the initial air temperature field. These tiny perturbations led to a randomization of the internal climate variability among the individual ensemble members (Figure 1), such that dominant modes of variability are out of phase within a decade or so. The CESM-ME ensemble members were each initialized from the corresponding historical simulation in CESM-LE (Figure 1) [*Sanderson et al.*, 2015]. A total of 38 (15) ensemble members were generated in this fashion for the CESM-LE (CESM-ME) experiment, though it was later discovered that ocean biogeochemical fields in six ensemble members from both CESM-LE and CESM-ME were corrupted due to an initialization error and could not be analyzed. All ensemble members have the same specified external forcing: historical forcing from 1920 to 2005 and either RCP8.5 or RCP4.5 forcing from 2006 onward.

McKinley et al. [2016] provide a thorough validation of the CESM-LE sea-air CO_2 flux in their manuscript (see their Figure 1, Extended Data Figure 1, and Extended Data Tables 1 and 2), so we highlight only the key points here. The simulated mean sea-air CO_2 flux from CESM-LE over 1982–2011 compares favorably to the flux estimated from observations [*Landschützer et al.*, 2014, 2015] for the global average and over most biomes. Two notable exceptions to this are the Southern Ocean marginal sea-ice biome, where CO_2 uptake in CESM-LE is too weak, and the East Pacific equatorial biome, where CO_2 outgassing in CESM-LE is too strong. The trends and interannual variability in modeled CO_2 flux over this period are largely consistent with those estimated by these same observations [*McKinley et al.*, 2016].

2.2. The CMIP5 Model Suite

The CESM ensembles are a tremendous numerical tool for assessing projection uncertainty due to internal variability and emission scenario. However, since these experiments include only a single climate model, they cannot address uncertainty arising from variation in model structure. To quantify this latter aspect of

Table 1. The CMIP5 Models Analyzed in This Study

CMIP5 Model	Ocean BGC Model	Reference	RCPs
BCC-CSM1.1	OCMIP	*Wu et al.* [2013]	8.5
CESM1-BGC	BEC	*Long et al.* [2013]	4.5, 8.5
CMCC-ESM	PELAGOS	*Vichi et al.* [2011]	8.5
GFDL-ESM2M	TOPAZ2	*Dunne et al.* [2013]	2.6, 4.5, 6.0, 8.5
HADGEM2-ES	Diat-HadOCC	*Collins et al.* [2011]	2.6, 4.5, 6.0, 8.5
IPSL-CM5A-MR	PISCES	*Dufresne et al.* [2013]	2.6, 4.5, 8.5
MIROC-ESM	NPZD	*Watanabe et al.* [2011]	2.6, 4.5, 6.0, 8.5
MPI-ESM-LR	HAMOCC	*Ilyina et al.* [2013]	2.6, 4.5, 8.5
NorESM1-ME	HAMOCC5	*Tjiputra et al.* [2013]	2.6, 4.5, 6.0, 8.5

uncertainty, we also analyze output from CMIP5. Under the protocols adopted for CMIP5, modeling centers performed a long, preindustrial control simulation (≥500 years) and two transient climate experiments: the first covers the period from 1850 to 2005, when the models were forced with a common set of historical anthropogenic forcings, while the second covers the period from 2006 to 2100 and is described by a collection of RCPs [*Taylor et al.*, 2012]. More than 20 modeling groups performed CMIP5 simulations, but only a subset of these included ocean biogeochemistry [*Taylor et al.*, 2012]. Table 1 shows the CMIP5 model simulations analyzed in this study. Note that not all modeling centers simulated all four emission scenarios. The CESM simulations included in CMIP5 were conducted with a different CESM configuration than that used in the CESM-LE and CESM-ME. In particular, the atmosphere component used for CMIP5 was the Community Atmosphere Model, version 4 (CAM4), while the CESM-LE/ME used CAM5. Also, the absorption of shortwave radiation in the ocean was computed using prognostic chlorophyll in the CMIP5 version [*Lindsay et al.*, 2014].

3. Results

3.1. Globally Integrated CO_2 Flux

Globally integrated, annual-mean sea-air CO_2 flux from CESM-LE, CESM-ME, and CMIP5 over 2006–2080 are shown in Figures 2a and 2b (thin lines). Negative numbers correspond to ocean uptake, and all global integrals were calculated on their native model grids. While all simulations indicate globally integrated ocean carbon uptake over this period, the magnitude of the projected uptake is clearly sensitive to emission scenario (multimodel mean for a given scenario shown as thick lines in Figures 2a and 2b) and model structure. The spread in global carbon uptake in the CMIP5 ensemble ranges from ~1 Pg C yr^{-1} at 2006 to 6 Pg C yr^{-1} in 2080.

To quantify uncertainty, we express an individual model solution as $T(m, s, t)$, which is the globally integrated or regional mean CO_2 flux as a function of model m, emission scenario s, and time t.

The uncertainty in globally integrated sea-air CO_2 flux can be quantified on the basis of ensemble spread, or the standard deviation of all the projections in a given year,

$$U(t) = \sqrt{var^{w}_{m,s}(T(m, s, t))}, \tag{1}$$

where $var^{w}_{m,s}$ is the weighted variance across all models and scenarios, using a weighting scheme that accounts for the number of ensemble members simulating each emission scenario. To compare uncertainty estimates derived from the CESM ensembles with those from CMIP5, we scale the respective metrics of model spread (equation (1)) by their weighted ensemble means,

$$U_{\mathrm{SCALED}}(t) = \frac{1.96 \cdot U(t)}{|\overline{T(m, s, t)}^{m,s}|} \tag{2}$$

where U_{SCALED} is the scaled uncertainty (95% confidence level, assuming a normal distribution), a unitless quantity, and $\overline{T(m, s, t)}^{m,s}$ is a weighted mean across all models and scenarios at a given time. Figures 2c and 2d show the scaled uncertainty in the projection of globally integrated sea-air CO_2 flux from the CESM ensembles and CMIP5, respectively. Uncertainty grows with prediction lead time in both model suites, and the uncertainty in CMIP5 is larger than that in the CESM ensembles at all lead times.

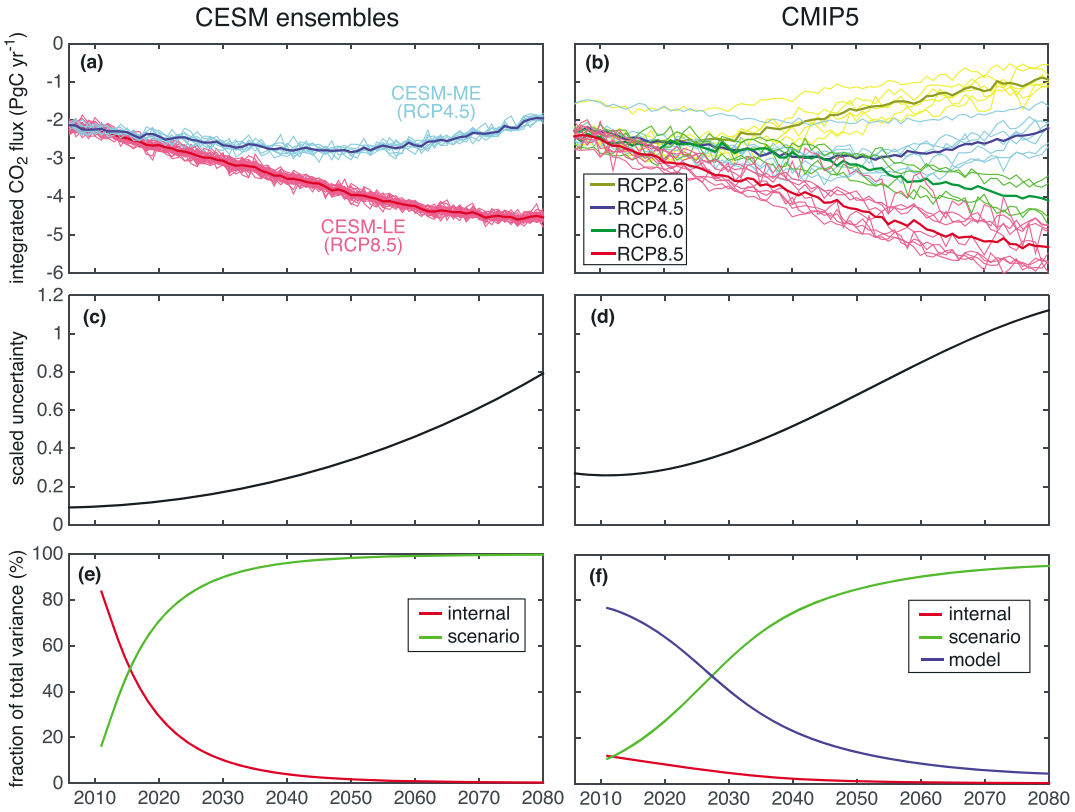

Figure 2. Annual-mean, globally integrated sea-air CO_2 flux projections (Pg C yr^{-1}) from the CESM ensembles and CMIP5, and the associated scaled uncertainty and sources of uncertainty in the projections.

We use the method outlined in *Hawkins and Sutton* [2009] and *Hawkins and Sutton* [2011] to isolate the three sources of projection uncertainty in air-sea CO_2 flux. The total variance, $U(t)^2$ is equal to the sum of the variance due to internal variability, U_V^2, the variance due to emission scenario, $U_S(t)^2$, and the variance due to model structure, $U_M(t)^2$,

$$U(t)^2 = U_V^2 + U_S(t)^2 + U_M(t)^2, \tag{3}$$

where we assume that the three sources of uncertainty are independent of each other, though one previous study suggests that this may not be strictly true because of small interaction between model and scenario uncertainties (see *Yip et al.* [2011] for further details).

The variance due to internal climate variability is calculated as

$$U_V^2 = \frac{\sum_{n=1}^{N_{em}} var_t(R(m,s,t))}{N_{em}}, \tag{4}$$

where var_t is the temporal variance, N_{em} is the total number of ensemble members in a given modeling suite, and $R(m,s,t)$ is a time series of residuals from the forced signal of climate change, $F(m,s,t)$,

$$R(m,s,t) = T(m,s,t) - F(m,s,t). \tag{5}$$

In the CESM ensembles, the forced signal is the ensemble mean for a given emission scenario and time, $F(s,t)$, smoothed with a 4th order polynomial fit to accommodate the different number of ensemble members for each scenario (i.e., to correct for the fact that the variance in the ensemble mean (thick lines in Figure 2a) is higher in CESM-ME than in CESM-LE owing to the different ensemble sizes). In the CMIP5 suite, the forced signal, $F(m,s,t)$, is estimated separately for each individual model projection by fitting a 4th order polynomial over the years 2006–2080. As in *Hawkins and Sutton* [2009], we make the assumption that the internal variance does not change with time and is unaffected by emission scenario.

The variance due to emission scenario is the cross-scenario variance of the multimodel mean forced signal:

$$U_S(t)^2 = var_s\left(\frac{\sum_{n=1}^{N_m} F(m,s,t)}{N_m}\right), \quad (6)$$

where N_m is the number of ensemble members in a given emission scenario.

The variance due to model structure is the multiscenario mean of the intermodel variance in the forced signal:

$$U_M(t)^2 = \frac{1}{N_s}\sum_{s=1}^{N_s} var_m(F(m,s,t)), \quad (7)$$

where N_s is the number of scenarios in a given model suite. In this statistical framework, the sum of the three uncertainty terms equals the total uncertainty, as derived by *Yip et al.* [2011] (see their equation (19), and note that we assume that the model-scenario interaction term is negligible).

Figures 2e and 2f show the fraction of the total variance due to each source of projection uncertainty in the globally integrated CO_2 flux, $\frac{U_V^2}{U(t)^2}$, $\frac{U_S(t)^2}{U(t)^2}$, and $\frac{U_M(t)^2}{U(t)^2}$ for internal variability, emission scenario, and model structure, respectively. In the CESM ensembles, where there are only two possible sources of projection uncertainty, we find that internal climate variability contributes to more than 50% of the variance for short prediction lead times (<2015), with emission scenario becoming the dominant source of uncertainty thereafter. By 2080, variance due to emission scenario is virtually 100% of the total variance. In the CMIP5 suite, model structural variance contributes to more than 50% of the total for short lead times (<2025), with emission scenario becoming the dominant source of variance thereafter. By 2080, variance due to emission scenario is >90% of the total. Internal climate variability contributes to less than 15% of the variance for all projection lead times in CMIP5. Since the internal variability is statistically indistinguishable between the CESM and CMIP5 model suites ($U^2_{V,\mathrm{CESM}} = 0.012 \pm 0.001$ (Pg C $yr^{-1})^2$; $U^2_{V,\mathrm{CMIP5}} = 0.016 \pm 0.006$ (Pg C $yr^{-1})^2$), the diminished fractional variability due to internal variance in CMIP5 is due the enhanced fractional variability in the other two sources of uncertainty. In CMIP5, the variance due to model structure nearly doubles from ~0.1 (Pg C $yr^{-1})^2$ in 2006 to ~0.2 (Pg C $yr^{-1})^2$ in 2080, due to differences in climate sensitivities across the models that manifest more strongly with increasing lead time. Nevertheless, results from our globally integrated CO_2 flux analysis with both modeling suites suggest that at lead times greater than 20 years, projection uncertainty is primarily driven by scenario uncertainty. As we will see in the next sections, this conclusion does not hold on regional scales.

3.2. Regional Focus: The California Current System

Studies assessing uncertainty in regional projections of temperature or precipitation find larger overall uncertainty and an enhanced role for internal variability, relative to projections at the global scale [*Hawkins and Sutton*, 2009, 2011; *Deser et al.*, 2016]. Here we illustrate this effect by quantifying the uncertainty partitioning for annual-mean sea-air CO_2 flux at a regional scale. We focus on the California Current System (pink area in Figure 3d inset), which is a region of particular interest for sea-air CO_2 flux projection, as ocean carbon uptake leads to ocean acidification, and previous studies document a high susceptibility to ocean acidification here [*Feely et al.*, 2008; *Gruber et al.*, 2012]. Further, this region is characterized by naturally high variability in carbonate chemistry which can affect future projections of acidification [*Hauri et al.*, 2013; *Leinweber and Gruber*, 2013; *Turi et al.*, 2016].

Figures 3a and 3b show projections of the annual-mean CO_2 flux from CESM-LE, CESM-ME, and the CMIP5 models averaged over the California Current System from 2006 to 2080. The California Current System is defined here as the region within 800 km of the coast and from ~33°N to 46°N [as in *Turi et al.*, 2014], and the regional averages are calculated on their native model grids, to capture near-shore values that might otherwise be masked with a regridding interpolation scheme. The CMCC-ESM showed highly unrealistic sea-air CO_2 flux values in this region; thus, we excluded it from our analysis of the CMIP5 suite. The individual projections (thin lines) from the CESM ensembles reveal ocean CO_2 uptake (negative numbers) for all ensemble members, but some CMIP5 ensemble members have a source of CO_2 during some periods. There is substantial overlap between integrations from different scenarios, suggesting only a small role for emission scenario in projection uncertainty in this region (Figures 3a and 3b).

The scaled uncertainty, $U_{\mathrm{SCALED}}(t)$, in California Current System sea-air CO_2 flux for the two modeling suites (Figures 3c and 3d) indicates larger uncertainty in this region, relative to the global scale for all projection lead

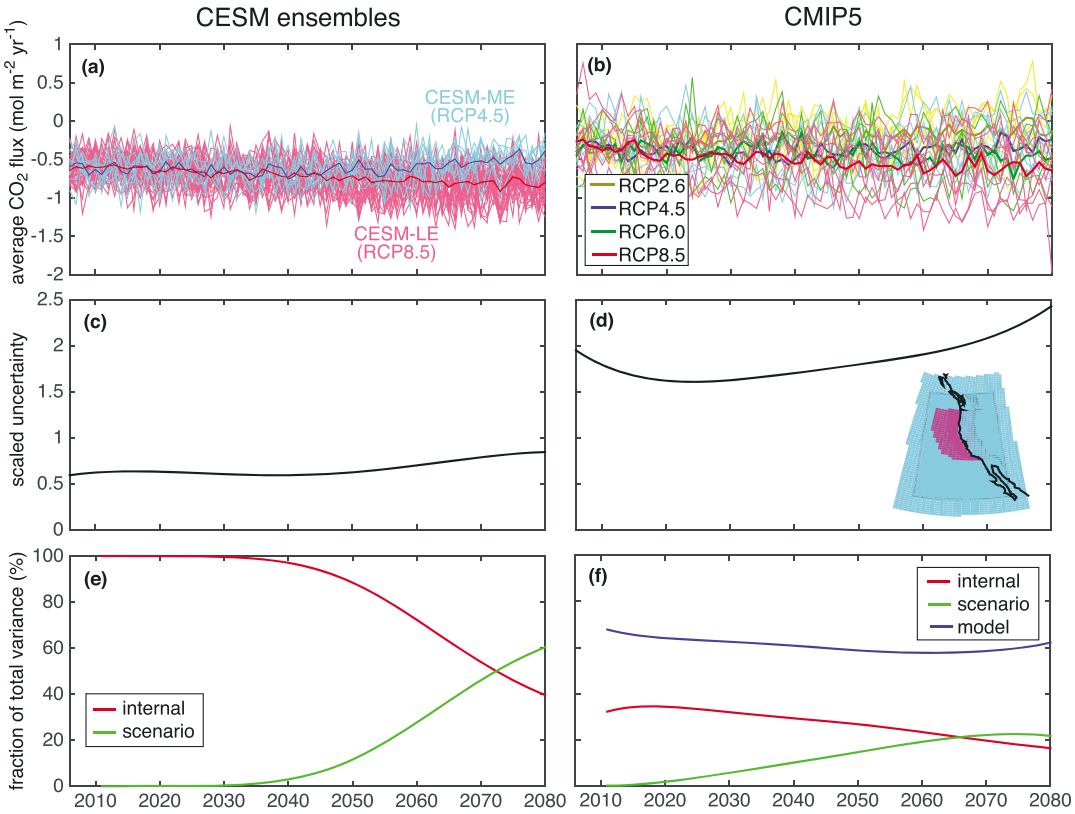

Figure 3. Annual-mean California Current System average sea-air CO_2 flux projections (mol C m^{-2} yr^{-1}) from the CESM ensembles and CMIP5, and the associated scaled uncertainty and sources of uncertainty in the projections. Inset in panel (d) shows a map of the California Current System region (pink).

times (cf. Figures 2c and 2d; note the different *y* axis). Whereas the globally integrated CO_2 flux uncertainty revealed growing uncertainty with higher prediction lead times, the California Current System CO_2 flux uncertainty only slightly increases with lead time in CMIP5 and remains relatively constant for all lead times in the CESM ensembles. As was the case at the global scale, the regional projection uncertainty in CMIP5 is larger than that in the CESM ensembles for all lead times.

We identify the sources of uncertainty in the California Current System regional-mean sea-air CO_2 flux projections (equations (3)–(7)) and show the results in Figures 3e and 3f, where the fraction of the total variance due to internal variability, emission scenario, and model structure are calculated separately for each model suite. In the CESM ensembles, we find that internal climate variability dominates the uncertainty until ~2070, with emission scenario playing a relatively small role. This is also visible in Figure 3a, where the CESM-LE and CESM-ME ensemble members exhibit some overlap for all lead times, and divergence between the two ensembles is not observed until the end of the time series. That nearly 100% of the uncertainty in the CESM ensembles is driven by internal climate variability until 2030 suggests an important role for internal climate variability in projections of CO_2 flux in this region for several decades. In the CMIP5 suite, model structure contributes to more than 60% of the total variance for all lead times, with internal variability playing a secondary role and emission scenario a tertiary role. We note that the relative fractional contributions of internal and scenario uncertainty in CMIP5 is similar to that observed in the CESM ensembles: internal climate variability drives a larger fraction of the uncertainty for all but the longest lead times. As was the case at the global scale, the internal variance in California Current System regional-mean CO_2 flux is similar between the two modeling suites ($U^2_{V,\mathrm{CESM}} = 0.044 \pm 0.002$ (mol m^{-2} $yr^{-1})^2$; $U^2_{V,\mathrm{CMIP5}} = 0.037 \pm 0.005$ (mol m^{-2} $yr^{-1})^2$), so the smaller fractional variability in internal variance in CMIP5 is due to the larger fractional variability in model structure. In summary, these results indicate that the high projection uncertainty observed in this region in the CESM ensembles (CMIP5 models) is largely driven by uncertainty in internal variability (model structure). Thus, at the regional scale, we have observed an important role for model structure and internal variability that was not evident in projection uncertainty at the global scale.

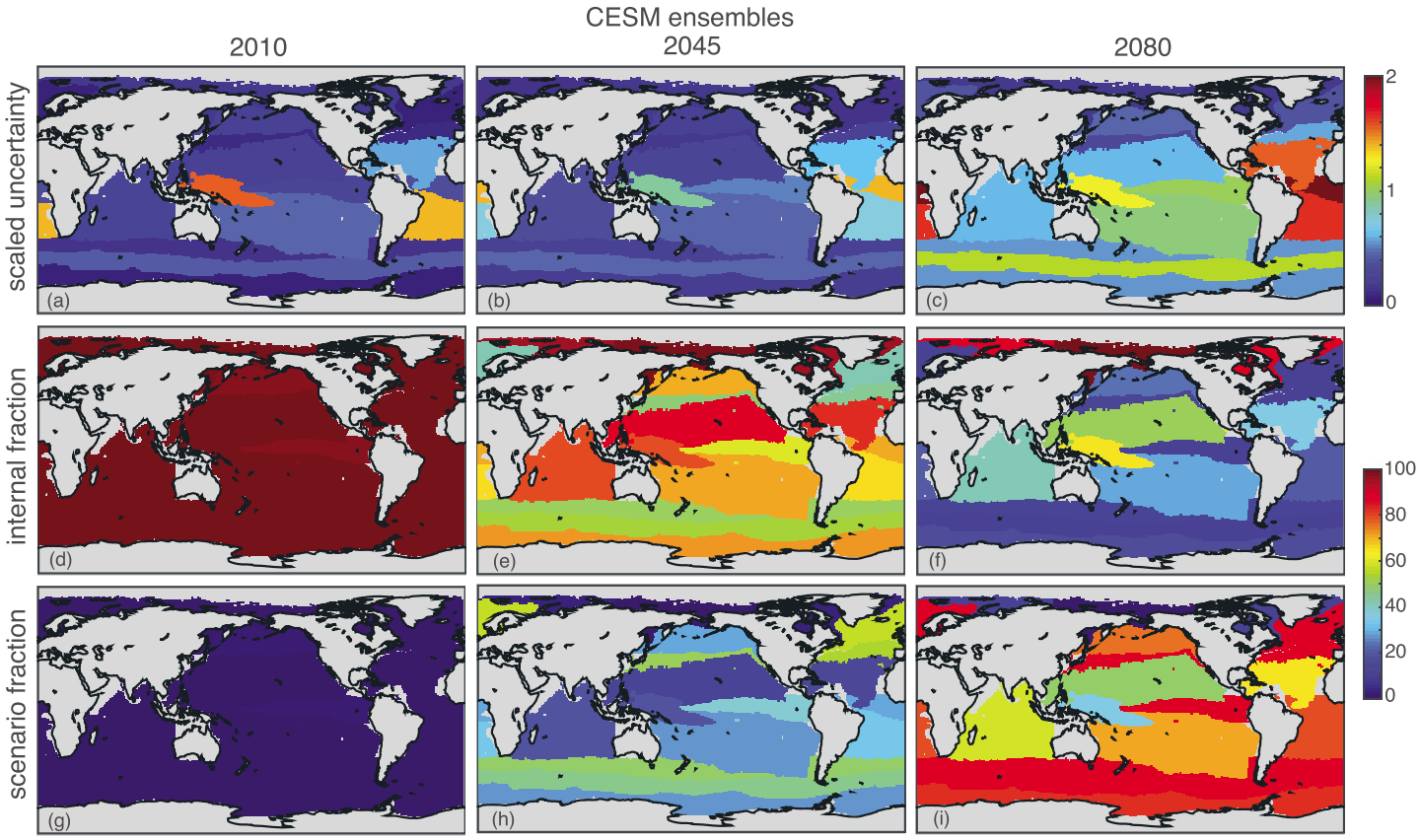

Figure 4. (first row) Scaled uncertainty in sea-air CO_2 flux projections and fractional variance (%) due to (second row) internal variability and (third row) emission scenario for each biome in (first column) 2010, (second column) 2045, and (third column) 2080 in the CESM ensembles.

3.3. Uncertainty on the Biome Scale

We quantify the regional uncertainty in sea-air CO_2 flux projections across the globe by averaging local CO_2 flux over 17 biogeographical biomes. This is achieved by regridding the fluxes from the model suites to a regular $1^\circ \times 1^\circ$ grid and then applying the mean biomes provided in *Fay and McKinley* [2014]. The scaled uncertainty, $U_{SCALED}(t)$, in the area-weighted CO_2 flux for each biome in the CESM ensembles is shown for three prediction lead time sin Figure 4. In 2010 (prediction lead time of 5 years), the scaled uncertainty ranges from near-zero in some biomes (e.g., the Southern Ocean seasonally ice-covered biome) to >1 in others (e.g., the west Pacific equatorial biome), indicating a spatially heterogenous pattern of uncertainty across the biomes. In 2045, the scaled uncertainty appears very similar to that of 2010, suggesting that uncertainty on the biome scale is relatively constant with prediction lead time, consistent with our findings in the California Current System. In 2080, most biomes show an increase in scaled uncertainty relative to 2045, with a few exceptions (e.g., the Northern Hemisphere seasonally ice-covered biome).

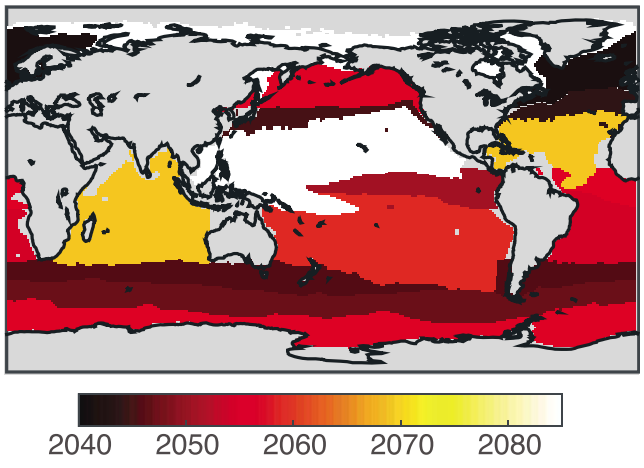

Figure 5. For each biome, the year when uncertainty due to emission scenario begins to dominate over uncertainty due to internal variability in the CESM ensembles.

In the CESM ensembles, there are only two sources of projection uncertainty:

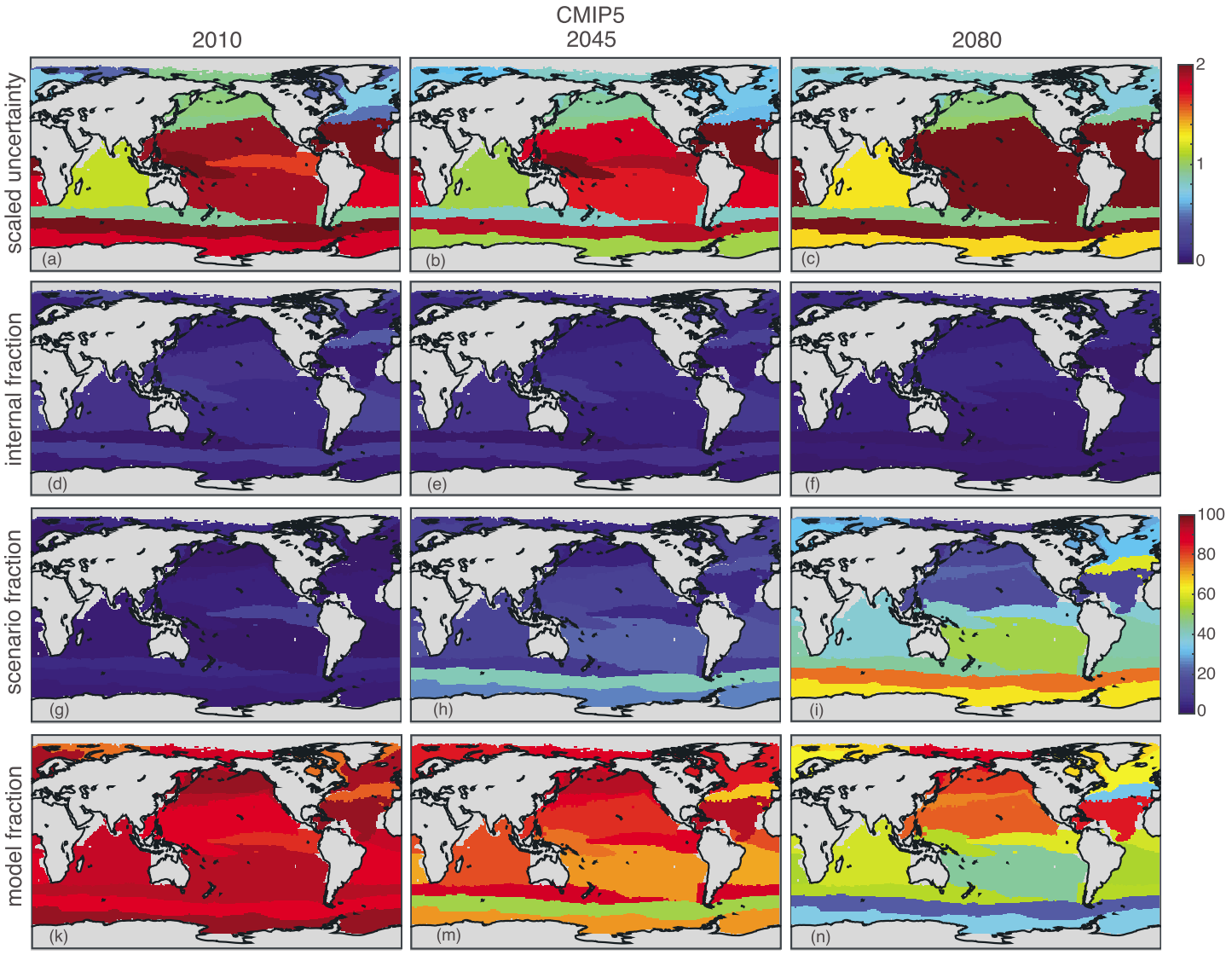

Figure 6. (first row) Scaled uncertainty in sea-air CO_2 flux projections and fractional variance (%) due to (second row) internal variability, (third row) emission scenario, and (fourth row) model structure for each biome in (first column) 2010, (second column) 2045, and (third column) 2080 in CMIP5.

internal variability and emission scenario. For each biome, we calculate the fraction of the total variance due to these two sources of uncertainty for all prediction lead times; Figures 4d–4i show the fractional contributions from the two uncertainty sources for 2010, 2045, and 2080. This analysis reveals that for each biome, internal variability dominates the uncertainty for medium-to-long prediction lead times, with emission scenario dominating the uncertainty thereafter. Figure 5 shows the year when uncertainty due to emission scenario begins to dominate over uncertainty due to internal variability in the CESM ensembles (i.e., the year when the red and green lines cross in a version of Figures 2e and 3e made for each biome). This analysis reveals that the crossover point is as early as 2040 in some biomes (e.g., Southern Ocean and North Atlantic subpolar seasonally stratified biomes), and later than 2080 in others (e.g., the west Pacific equatorial biome). The spatial pattern associated with the crossover point (Figure 5) is quite similar to that of anthropogenic CO_2 uptake [*DeVries*, 2014]: places with high anthropogenic CO_2 uptake over the historical period (e.g., North Atlantic and Southern Ocean) have early crossover times. Here the emission scenario is the most important source of projection uncertainty earlier than in other regions. It is important to note that Figure 5 is fundamentally different from "time of emergence" (ToE) maps that are percolating into the ocean biogeochemical literature

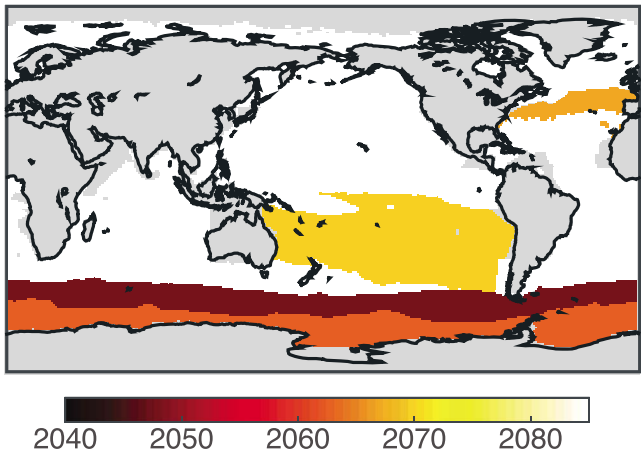

Figure 7. For each biome, the year when uncertainty due to emission scenario begins to dominate over uncertainty due to model structure in CMIP5.

[*Keller et al.*, 2014; *Rodgers et al.*, 2015; *Lovenduski et al.*, 2015b; *Henson et al.*, 2016; *McKinley et al.*, 2016]. ToE indicates when a trend will emerge from background variability but provides little information about the sources of projection uncertainty.

The scaled uncertainty in the biome-averaged sea-air CO_2 flux in the CMIP5 models is shown in Figure 6. This analysis reveals high uncertainty for short-to-medium prediction lead times over most biomes (Figures 6a and 6b). As in the CESM ensembles, the longest prediction lead times are associated with the highest uncertainty (Figure 6c). The fraction of the total variance due to model structural uncertainty is large in all biomes, with internal variability and emission scenario contributing to only a small fraction of the variance (Figures 6d – 6n) and is the dominant source of projection uncertainty for all lead times in all but four of the biomes (Figure 7). Thus, our analysis of projection uncertainty in the CMIP5 suite on the biome scale suggests an important role for model structure, consistent with our findings in the California Current System.

4. Conclusions

We analyze output from the CESM ensembles and the CMIP5 suite to quantify the projection uncertainty in sea-air CO_2 flux and to partition the projection uncertainty into its three main sources: internal variability, emission scenario, and model structure. We find that projections of sea-air CO_2 flux exhibit high uncertainty, particularly at regional scales and for long prediction lead times. The three sources of projection uncertainty vary with prediction lead time, spatial averaging scale, and from region to region. Uncertainty in globally integrated CO_2 flux projections from both model suites is dominated by emission scenario for nearly all prediction lead times. In the California Current System and over most ocean biomes, the dominant sources of projection uncertainty are internal variability and model structure for the CESM ensemble and the CMIP5 suite, respectively, with emission scenario playing only a small role in all but a few biomes.

We note that while the CESM ensembles provide a robust estimate of internal climate variability, the same cannot be said about the CMIP5 model suite. Most modeling centers provided only one realization of the future climate system to the CMIP5 archive for each emission scenario, and internal variability in these models is therefore estimated via the residuals from a polynomial fit to the CO_2 flux time series. Further, the internal variability signal is averaged across all ensemble members in order to estimate the uncertainty, yet a previous study has shown that internal variability in CO_2 flux varies from model to model [*Resplandy et al.*, 2015]. Additionally, we assume here that internal variability in CO_2 flux does not change with time and is unaffected by emission scenario. While this assumption may be valid for projections of atmospheric temperature [*Thompson et al.*, 2015], it has not yet been tested for the nonlinear ocean carbonate chemistry system. Further investigation is thus merited on these topics. For ocean CO_2 flux, one possible route forward is a comparison of output from multiple large initial condition ensemble experiments [e.g., *Schlunegger et al.*, 2016].

Where should we invest our resources so as to reduce uncertainty in sea-air CO_2 flux projections? Our results point to a clear role for model structural uncertainty in regional projections of sea-air CO_2 flux and suggest that improvements to model structure will significantly reduce the projection uncertainty on these scales.

One possible route to successful prediction would be to devise a weighting scheme for models based on their skill at producing historical observations [*Hawkins and Sutton*, 2009], though observational estimates of sea-air CO_2 flux are few [e.g., *Landschützer et al.*, 2014; *Rödenbeck et al.*, 2014], and we would expect different models to have varying degrees of predictive skill over different regions. At the very least, the impact of structural differences on the modeled CO_2 fluxes should be explored in more detail, and the next generation of CMIP models should be evaluated to see if model structural uncertainty has been reduced. Our findings also suggest that internal climate variability plays an important role in projection uncertainty on regional scales, but given the aleatoric nature of the climate system, reductions in this source of uncertainty seem unlikely. Finally, given the important role of emission scenario uncertainty in sea-air CO_2 flux projections both globally and in some regions (e.g., the North Atlantic and Southern Oceans), efforts to narrow this source of uncertainty would go a long way toward improving projections here.

Acknowledgments
CESM ensemble output is available from the Earth System Grid (https://www.earthsystemgrid.org/dataset/ucar.cgd.ccsm4.CESM_CAM5_BGC_LE.html and https://www.earthsystemgrid.org/dataset/ucar.cgd.ccsm4.CESM_CAM5_BGC_ME.html). CESM computing resources were provided by CISL at NCAR. CMIP5 output was provided by the World Data Center for Climate (http://cera-www.dkrz.de). NCAR is sponsored by NSF. We are grateful for funding from NSF (OCE-1558225 and OCE-1155240), NOAA (NA12OAR4310058), and NASA (NNX11AF53G and NNX13AC53G).

References

Arora, V. K., et al. (2013), Carbon-concentration and carbon-climate feedbacks in CMIP5 Earth system models, *J. Clim.*, *26*(15), 5289–5314, doi:10.1175/JCLI-D-12-00494.1.

Ciais, P., and C. Sabine (2013), Chapter 6: Carbon and other biogeochemical cycles, in *Climate Change 2013: The Physical Science Basis. Contribution of Working Group I to the Fifth Assessment Report of the Intergovernmental Panel on Climate Change*, edited by T. F. Stocker et al., p. 1535, Cambridge Univ. Press, Cambridge, U. K., and New York.

Collins, W. J., et al. (2011), Development and evaluation of an Earth-System model—HadGEM2, *Geosci. Model Dev.*, *4*(4), 1051–1075, doi:10.5194/gmd-4-1051-2011.

Danabasoglu, G., S. C. Bates, B. P. Briegleb, S. R. Jayne, M. Jochum, W. G. Large, S. Peacock, and S. G. Yeager (2012), The CCSM4 ocean component, *J. Clim.*, *25*(5), 1361–1389.

Deser, C., L. Terray, and A. S. Phillips (2016), Forced and internal components of winter air temperature trends over North America during the past 50 years: Mechanisms and implications, *J. Clim.*, *29*, 2237–2258, doi:10.1175/JCLI-D-15-0304.1.

DeVries, T. (2014), The oceanic anthropogenic CO_2 sink: Storage, air-sea fluxes, and transports over the industrial era, *Global Biogeochem. Cycles*, *28*(7), 631–647, doi:10.1002/2013GB004739.

Doney, S. C., K. Lindsay, I. Fung, and J. John (2006), Natural variability in a stable, 1000-yr global coupled climate–carbon cycle Simulation, *J. Clim.*, *19*(13), 3033–3054.

Dufresne, J.-L., et al. (2013), Climate change projections using the IPSL-CM5 Earth System Model: From CMIP3 to CMIP5, *Clim. Dyn.*, *40*(9), 2123–2165, doi:10.1007/s00382-012-1636-1.

Dunne, J. P., et al. (2013), GFDL's ESM2 global coupled climate-carbon Earth System Models. Part II: Carbon system formulation and baseline simulation characteristics, *J. Clim.*, *26*(7), 2247–2267, doi:10.1175/JCLI-D-12-00150.1.

Fay, A. R., and G. A. McKinley (2014), Global open-ocean biomes: Mean and temporal variability, *Earth Syst. Sci. Data*, *6*(2), 273–284, doi:10.5194/essd-6-273-2014.

Feely, R. A., C. L. Sabine, J. M. Hernandez-Ayon, D. Ianson, and B. Hales (2008), Evidence for upwelling of corrosive "acidified" water onto the continental shelf, *Science*, *320*(5882), 1490–1492, doi:10.1126/science.1155676.

Fox-Kemper, B., G. Danabasoglu, R. Ferrari, S. Griffies, R. Hallberg, M. Holland, M. Maltrud, S. Peacock, and B. Samuels (2011), Parameterization of mixed layer eddies. III: Implementation and impact in global ocean climate simulations, *Ocean Modell.*, *39*(1–2), 61–78.

Friedrich, T., et al. (2012), Detecting regional anthropogenic trends in ocean acidification against natural variability, *Nat. Clim. Change*, *2*(3), 167–171.

Frölicher, T. L., F. Joos, G.-K. Plattner, M. Steinacher, and S. C. Doney (2009), Natural variability and anthropogenic trends in oceanic oxygen in a coupled carbon cycle–climate model ensemble, *Global Biogeochem. Cycles*, *23*, GB1003, doi:10.1029/2008GB003316.

Frölicher, T. L., J. L. Sarmiento, D. J. Paynter, J. P. Dunne, J. P. Krasting, and M. Winton (2014), Dominance of the Southern Ocean in anthropogenic carbon and heat uptake in CMIP5 models, *J. Clim.*, *28*(2), 862–886, doi:10.1175/JCLI-D-14-00117.1.

Frölicher, T. L., K. B. Rodgers, C. Stock, and W. W. L. Cheung (2016), Sources of uncertainties in 21st century projections of potential ocean ecosystem stressors, *Global Biogeochem. Cycles*, doi:10.1002/2015GB005338.

Gent, P. R., and J. C. McWilliams (1990), Isopycnal mixing in ocean circulation models, *J. Phys. Oceanogr.*, *20*(1), 150–155.

Gruber, N., C. Hauri, Z. Lachkar, D. Loher, T. L. Frölicher, and G.-K. Plattner (2012), Rapid progression of ocean acidification in the California Current System, *Science*, *337*(6091), 220–223, doi:10.1126/science.1216773.

Hauck, J., et al. (2015), On the Southern Ocean CO_2 uptake and the role of the biological carbon pump in the 21st century, *Global Biogeochem. Cycles*, *29*, 1451–1470, doi:10.1002/2015GB005140.

Hauri, C., N. Gruber, M. Vogt, S. C. Doney, R. A. Feely, Z. Lachkar, A. Leinweber, A. M. P. McDonnell, M. Munnich, and G.-K. Plattner (2013), Spatiotemporal variability and long-term trends of ocean acidification in the California Current System, *Biogeosciences*, *10*(1), 193–216, doi:10.5194/bg-10-193-2013.

Hawkins, E., and R. Sutton (2009), The potential to narrow uncertainty in regional climate predictions, *Bull. Am. Meteorol. Soc.*, *90*(8), 1095–1107, doi:10.1175/2009BAMS2607.1.

Hawkins, E., and R. Sutton (2011), The potential to narrow uncertainty in projections of regional precipitation change, *Clim. Dyn.*, *37*(1–2), 407–418, doi:10.1007/s00382-010-0810-6.

Henson, S. A., C. Beaulieu, and R. Lampitt (2016), Observing climate change trends in ocean biogeochemistry: When and where, *Global Change Biol.*, *22*(4), 1561–1571, doi:10.1111/gcb.13152.

Holland, M. M., D. A. Bailey, B. P. Briegleb, B. Light, and E. Hunke (2012), Improved sea ice shortwave radiation physics in CCSM4: The impact of melt ponds and aerosols on Arctic sea ice, *J. Clim.*, *25*(5), 1413–1430, doi:10.1175/JCLI-D-11-00078.1.

Hunke, E. C., and W. H. Lipscomb (2008), CICE: the Los Alamos sea ice model user's manual, version 4, Tech. Rep. LA-CC-06-012, Los Alamos Natl. Lab., Los Alamos, N. M.

Ilyina, T., K. D. Six, J. Segschneider, E. Maier-Reimer, H. Li, and I. Núñez-Riboni (2013), Global ocean biogeochemistry model HAMOCC: Model architecture and performance as component of the MPI-Earth system model in different CMIP5 experimental realizations, *J. Adv. Model. Earth Syst.*, *5*(2), 287–315, doi:10.1029/2012MS000178.

Kay, J. E., et al. (2015), The Community Earth System Model (CESM) Large Ensemble project: A community resource for studying climate change in the presence of internal climate variability, *Bull. Am. Meteorol. Soc.*, *96*(8), 1333–1349, doi:10.1175/BAMS-D-13-00255.1.
Keller, K. M., F. Joos, and C. C. Raible (2014), Time of emergence of trends in ocean biogeochemistry, *Biogeosciences*, *11*(13), 3647–3659, doi:10.5194/bg-11-3647-2014.
Landschützer, P., N. Gruber, D. C. E. Bakker, and U. Schuster (2014), Recent variability of the global ocean carbon sink, *Global Biogeochem. Cycles*, *28*, 927–949, doi:10.1002/2014GB004853.
Landschützer, P., et al. (2015), The reinvigoration of the Southern Ocean carbon sink, *Science*, *349*(6253), 1221–1224.
Large, W. G., J. C. McWilliams, and S. C. Doney (1994), Oceanic vertical mixing: A review and a model with a nonlocal boundary layer parameterization, *Rev. Geophys.*, *32*(4), 363–403.
Laufkötter, C., et al. (2015), Drivers and uncertainties of future global marine primary production in marine ecosystem models, *Biogeosciences*, *12*, 6955–6984, doi:10.5194/bg-12-6955-2015.
Lawrence, D. M., K. W. Oleson, M. G. Flanner, C. G. Fletcher, P. J. Lawrence, S. Levis, S. C. Swenson, and G. B. Bonan (2012), The CCSM4 land simulation, 1850–2005: Assessment of surface climate and new capabilities, *J. Clim.*, *25*(7), 2240–2260, doi:10.1175/JCLI-D-11-00103.1.
Leinweber, A., and N. Gruber (2013), Variability and trends of ocean acidification in the Southern California Current System: A time series from Santa Monica Bay, *J. Geophys. Res. Oceans*, *118*, 3622–3633, doi:10.1002/jgrc.20259.
Lindsay, K., G. B. Bonan, S. C. Doney, F. M. Hoffman, D. M. Lawrence, M. C. Long, N. M. Mahowald, J. Keith Moore, J. T. Randerson, and P. E. Thornton (2014), Preindustrial-control and twentieth-century carbon cycle experiments with the Earth System Model CESM1(BGC), *J. Clim.*, *27*(24), 8981–9005, doi:10.1175/JCLI-D-12-00565.1.
Long, M. C., K. Lindsay, S. Peacock, J. K. Moore, and S. C. Doney (2013), Twentieth-century oceanic carbon uptake and storage in CESM1(BGC), *J. Clim.*, *26*(18), 6775–6800, doi:10.1175/JCLI-D-12-00184.1.
Long, M. C., C. Deutsch, and T. Ito (2016), Finding forced trends in oceanic oxygen, *Global Biogeochem. Cycles*, *30*, 381–397, doi:10.1002/2015GB005310.
Lovenduski, N. S., A. R. Fay, and G. A. McKinley (2015a), Observing multidecadal trends in Southern Ocean CO_2 uptake: What can we learn from an ocean model?, *Global Biogeochem. Cycles*, *29*(4), 416–426, doi:10.1002/2014GB004933.
Lovenduski, N. S., M. C. Long, and K. Lindsay (2015b), Natural variability in the surface ocean carbonate ion concentration, *Biogeosciences*, *12*(21), 6321–6335, doi:10.5194/bg-12-6321-2015.
McKinley, G. A., D. J. Pilcher, A. R. Fay, K. Lindsay, M. C. Long, and N. S. Lovenduski (2016), Timescales for detection of trends in the ocean carbon sink, *Nature*, *530*(7591), 469–472.
Meinshausen, M., et al. (2011), The RCP greenhouse gas concentrations and their extensions from 1765 to 2300, *Clim. Change*, *109*(1), 213–241, doi:10.1007/s10584-011-0156-z.
Moore, J. K., and O. Braucher (2008), Sedimentary and mineral dust sources of dissolved iron to the world ocean, *Biogeosciences*, *5*(3), 631–656.
Moore, J. K., S. C. Doney, and K. Lindsay (2004), Upper ocean ecosystem dynamics and iron cycling in a global three-dimensional model, *Global Biogeochem. Cycles*, *18*, GB4028, doi:10.1029/2004GB002220.
Moore, J. K., K. Lindsay, S. C. Doney, M. C. Long, and K. Misumi (2013), Marine ecosystem dynamics and biogeochemical cycling in the Community Earth System Model [CESM1(BGC)]: Comparison of the 1990s with the 2090s under the RCP4.5 and RCP8.5 scenarios, *J. Clim.*, *26*(23), 9291–9312, doi:10.1175/JCLI-D-12-00566.1.
Resplandy, L., R. Séférian, and L. Bopp (2015), Natural variability of CO_2 and O_2 fluxes: What can we learn from centuries-long climate models simulations?, *J. Geophys. Res. Oceans*, *120*, 384–404, doi:10.1002/2014JC010463.
Rödenbeck, C., D. C. E. Bakker, N. Metzl, A. Olsen, C. Sabine, N. Cassar, F. Reum, R. F. Keeling, and M. Heimann (2014), Interannual sea-air CO_2 flux variability from an observation-driven ocean mixed-layer scheme, *Biogeosciences*, *11*(17), 4599–4613, doi:10.5194/bg-11-4599-2014.
Rodgers, K. B., J. Lin, and T. L. Frölicher (2015), Emergence of multiple ocean ecosystem drivers in a large ensemble suite with an earth system model, *Biogeosciences*, *12*(11), 3301–3320, doi:10.5194/bg-12-3301-2015.
Roy, T., L. Bopp, M. Gehlen, B. Schneider, P. Cadule, T. L. Frölicher, J. Segschneider, J. Tjiputra, C. Heinze, and F. Joos (2011), Regional impacts of climate change and atmospheric CO_2 on future ocean carbon uptake: A multimodel linear feedback analysis, *J. Clim.*, *24*(9), 2300–2318, doi:10.1175/2010JCLI3787.1.
Sanderson, B. M., K. W. Oleson, W. G. Strand, F. Lehner, and B. C. O'Neill (2015), A new ensemble of GCM simulations to assess avoided impacts in a climate mitigation scenario, *Clim. Change*, 1–16, doi:10.1007/s10584-015-1567-z.
Schlunegger, S., K. B. Rodgers, J. L. Sarmiento, and T. L. Frölicher (2016), Using initial condition large ensemble experiments to interpret observed trends and 21^{st} century projections of ocean carbon uptake, *paper presented at Ocean Sciences Meeting*, PC44B–2198, AGU, New Orleans, La., 21–26 Feb.
Taylor, K. E., R. J. Stouffer, and G. A. Meehl (2012), An overview of CMIP5 and the experiment design, *Bull. Am. Meteorol. Soc.*, *93*(4), 485–498, doi:10.1175/BAMS-D-11-00094.1.
Thompson, D. W. J., E. A. Barnes, C. Deser, W. E. Foust, and A. S. Phillips (2015), Quantifying the role of internal climate variability in future climate trends, *J. Clim.*, *28*(16), 6443–6456, doi:10.1175/JCLI-D-14-00830.1.
Tjiputra, J. F., C. Roelandt, M. Bentsen, D. M. Lawrence, T. Lorentzen, J. Schwinger, Ø. Seland, and C. Heinze (2013), Evaluation of the carbon cycle components in the Norwegian Earth System Model (NorESM), *Geosci. Model Dev.*, *6*(2), 301–325, doi:10.5194/gmd-6-301-2013.
Tjiputra, J. F., A. Olsen, L. Bopp, A. Lenton, B. Pfeil, T. Roy, J. Segschneider, I. Totterdell, and C. Heinze (2014), Long-term surface pCO_2 trends from observations and models, *Tellus B*, *66*, 23083, doi:10.3402/tellusb.v66.23083.
Turi, G., Z. Lachkar, and N. Gruber (2014), Spatiotemporal variability and drivers of pCO_2 and air-sea CO_2 fluxes in the California Current System: An eddy-resolving modeling study, *Biogeosciences*, *11*(3), 671–690, doi:10.5194/bg-11-671-2014.
Turi, G., Z. Lachkar, N. Gruber, and M. Münnich (2016), Climatic modulation of recent trends in ocean acidification in the California Current System, *Environ. Res. Lett.*, *11*(1), 14007.
Vichi, M., E. Manzini, P. G. Fogli, A. Alessandri, L. Patara, E. Scoccimarro, S. Masina, and A. Navarra (2011), Global and regional ocean carbon uptake and climate change: Sensitivity to a substantial mitigation scenario, *Clim. Dyn.*, *37*(9), 1929–1947, doi:10.1007/s00382-011-1079-0.
Watanabe, S., et al. (2011), MIROC-ESM 2010: Model description and basic results of CMIP5-20c3m experiments, *Geosci. Model Dev.*, *4*(4), 845–872, doi:10.5194/gmd-4-845-2011.
Wu, T., et al. (2013), Global carbon budgets simulated by the Beijing Climate Center Climate System Model for the last century, *J. Geophys. Res. Atmos.*, *118*, 4326–4347, doi:10.1002/jgrd.50320.
Yip, S., C. A. T. Ferro, D. B. Stephenson, and E. Hawkins (2011), A simple, coherent framework for partitioning uncertainty in climate predictions, *J. Clim.*, *24*(17), 4634–4643, doi:10.1175/2011JCLI4085.1.